A SIMPLIFIED MODEL OF JET FORMATION IN HEMISPHERICAL SHAPED CHARGES

PEI CHI CHOU; WILLIAM J. FLIS; COLIN M. FORSYTH
Dyna East Corporation
Philadelphia, PA U.S.A.

Presented is a simplified model of jet formation of shaped charges with hemispherical liners. First, the shape and velocity of the jet are expressed as functions of the liner's total momentum and kinetic energy. Then, a formula is proposed for the liner's collapse velocity, based on a combination of the Gurney formulas for plate acceleration and cylindrical implosion. This velocity is integrated over the liner to yield its total momentum and energy, and hence determine the properties of the resulting jet.

INTRODUCTION

This paper presents a simple model of the jet-formation process in shaped charges with hemispherical liners. It is a continuation of the work reported in [1], [2] and [3]. In [1], an implosively loaded hemispherical liner was simulated by the two-dimensional computer code HELP, and the results were compared with those of the implosively loaded case. It was shown that the formation of jets from the three types of liners, namely, implosively loaded hemisphere, point-initiated hemisphere, and cones, are all different. In [1] and [2], liner material flow was analyzed in detail, but specific models, from which quantitative calculation and prediction can be made, were not offered.

Physical models with simple equations are needed. Even though computer codes yield detailed information, they are time-consuming, and their results are difficult to analyze. Physical models offer more insight into formation mechanisms, and are easy to use. For conical shaped charges, the well-known P-E-R model [5] gives an accurate picture of the formation mechanism and has been used widely.

Few models for hemispherical liners have been offered in the past. Reference [6] gave a simple jet-formation model based on the assumption that a liner element (of a circular ring shape) forms a single solid cylindrical jet element of constant velocity (see Figure 6 of [6]). An element through the liner thickness at the hemisphere's apex forms the jet tip, and the tip velocity is calculated from this element alone, without interaction with other liner elements. It is clear from the computer-code simulations of [1] and [2] that their assumptions are overly simplified.

In this paper, a simplified model of jet formation for hemispherical shaped charges is presented. This model has two main parts. In the first part, jet tip and tail velocities are expressed as explicit functions of total liner momentum and kinetic energy. In the second part, a formula for the liner collapse velocity is proposed, which can be used to determine the liner's momentum and energy.

We first present the development of these two parts of the theory. Results of the model are then compared with code simulations and experiments. Finally, parametric calculations with the model show that it correctly predicts trends due to variations in liner thickness and liner tapering.

THEORY

Observation of radiographs show shows that the radius and velocity of jets from hemispherical liners

usually both have linear variations along the length. For simplicity, the jet is assumed to have the shape of a truncated cone and a linear distribution of velocity along its length as shown in Figure 1. The accuracy of this assumption is demonstrated in Figure 2, which presents a grid plot from a DEFEL simulation of a hemispherical shaped charge. The linearity of the jet velocity was more fully demonstrated in [3], and the linearity of the radius is discussed in [2].

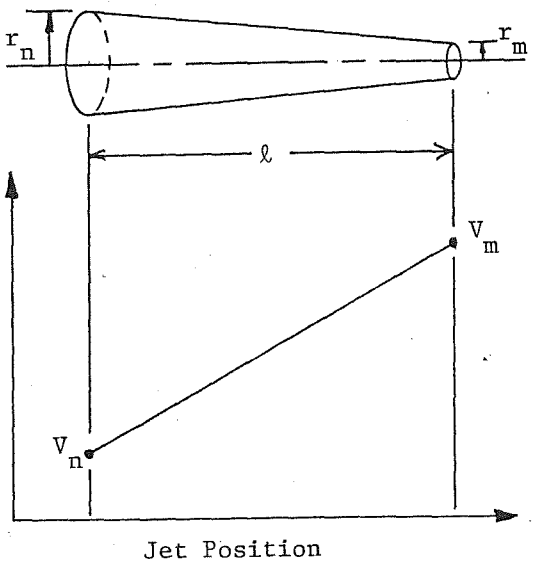

Figure 1. Linear Distributions of Jet Radius and Velocity, as Assumed in the Model.

The jet can then be completely described by specifying four properties: the velocities and radii of its tip and tail. These properties can be determined by four input quantities. Three of the inputs could be the total mass, axial momentum, and kinetic energy of the collapsing liner. Under these conditions, the mass, axial momentum, and kinetic energy of the jet may be expressed as:

$$M = \frac{1}{3}\rho\pi\ell r_n^2 (p^2 + p + 1) \qquad (1)$$

$$P = \frac{1}{12}\rho\pi\ell r_n^2 [(3p^2 + 2p + 1)V_m + (p^2 + 2p + 3)V_n] \qquad (2)$$

$$E = \frac{1}{60}\rho\pi\ell r_n^2 [(6p^2 + 3p + 1)V_m^2 + (3p^2 + 4p + 3)V_m V_n + (p^2 + 3p + 6)V_n^2] \qquad (3)$$

where

$$p = \frac{r_m}{r_n}$$

and

ℓ = jet length
r_m = tip radius
r_n = tail radius
V_m = tip velocity
V_n = tail velocity

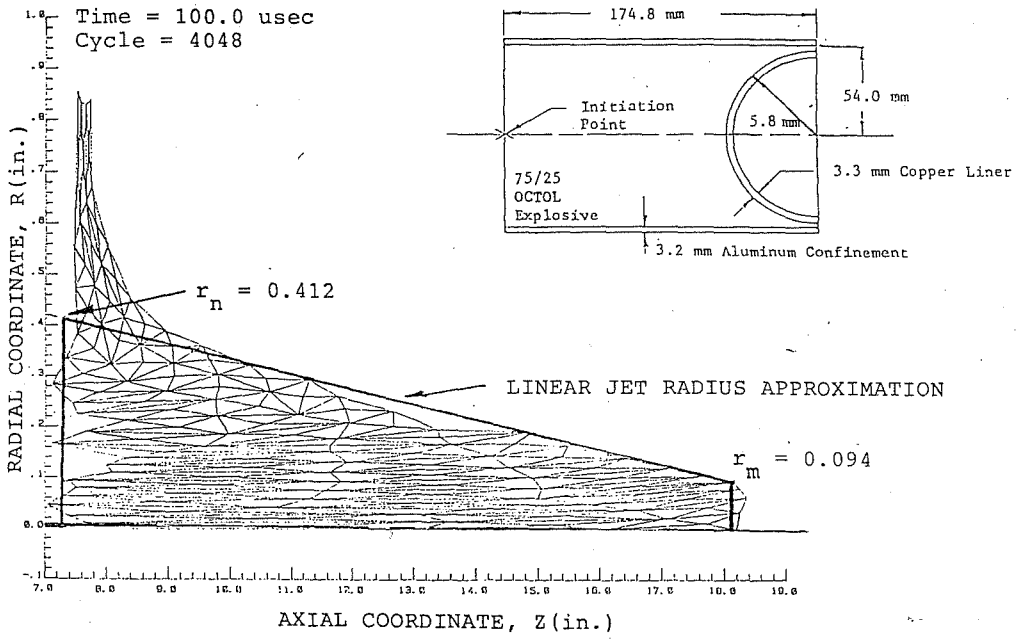

Figure 2. Finite-element Grid of Jet Projected by the Charge Shown, as Calculated by the DEFEL Code.

If the mass, momentum, and energy of a collapsing liner are given, then the above equations are insufficient to determine all four variables that describe the jet's velocity distribution and shape. However, if the ratio of the tip and tail radii is known, these three equations may be inverted to give expressions of the velocities and radii in terms of the mass, momentum, and energy. Thus, the above equations may be rearranged to yield:

$$\frac{V_m}{V_{CG}} = \left(\frac{2p_1}{3p_2} + \frac{p_3 K_2}{2p_2 K_1}\right) + \frac{p3}{p2} A \qquad (4)$$

$$\frac{V_n}{V_{CG}} = -\frac{K_2}{2K_1} - A \qquad (5)$$

$$r_n{}^2 \ell = \frac{3M}{\rho\pi} \frac{1}{p_1} \qquad (6)$$

in which

$$A = \left[\frac{K_2{}^2 - 4K_1K_3}{4K_1{}^2} + \frac{5p_1}{3K_1}\left(\frac{E}{1/2\ MV_{CG}{}^2}\right)\right]^{1/2}$$

$$p_1 = p^2 + p + 1$$

$$p_2 = \frac{p^2}{2} + \frac{p}{3} + \frac{1}{6}$$

$$p_3 = \frac{p^2}{6} + \frac{p}{3} + \frac{1}{2}$$

$$p_4 = p^2 + \frac{p}{2} + \frac{1}{6}$$

$$p_5 = \frac{p^2}{2} + \frac{2p}{3} + \frac{1}{2}$$

$$p_6 = \frac{p^2}{6} + \frac{p}{2} + 1$$

$$K_1 = \frac{p_3 p_5}{p^2} + p_6 + \frac{p3^2 p4}{p_2{}^2}$$

$$K_2 = \frac{4p_1 p_3 p_4}{3p_2{}^2} + \frac{2}{3}\frac{p_1 p_5}{p_2}$$

$$K_3 = \frac{4p_4 p_1{}^2}{9p_2{}^2}$$

and $V_{CG} = P/M$ is velocity of the center of mass of the jet. Given the jet mass M, axial momentum P, kinetic energy E, and radius p, the jet's tip and tail velocities and radii may be computed from these equations.

Note that the expressions for jet velocity, Equations (4) and (5), depend on the jet radii only through their ratio, $p = r_m/r_n$. That is, the velocities are independent of the scale of the jet, as expected. If we assume a value for the radius ratio p, then the tip and tail velocities of all possible jets may be given by a single curve.

Such a plot is given in Figure 3 for a value of p = 0.25. Observation of jet radiographs and the results of hydrocode simulations indicates that this value is a good approximation. Ratios of the tip and tail velocities to the average velocity are plotted versus the energy ratio $E/\frac{1}{2}MV_{CG}{}^2$. The value of the energy ratio reflects the rate of jet stretching. For an energy ratio equal to unity, $V_m = V_n = V_{CG}$, and there is no stretching at all. For a given V_{CG}, greater energy indicates a larger difference between V_m and V_n, and a higher stretching rate. For a 42° conical charge, V_{CG} is high (5.24 km/s); therefore, the actual stretching is high, even though the energy ratio is small.

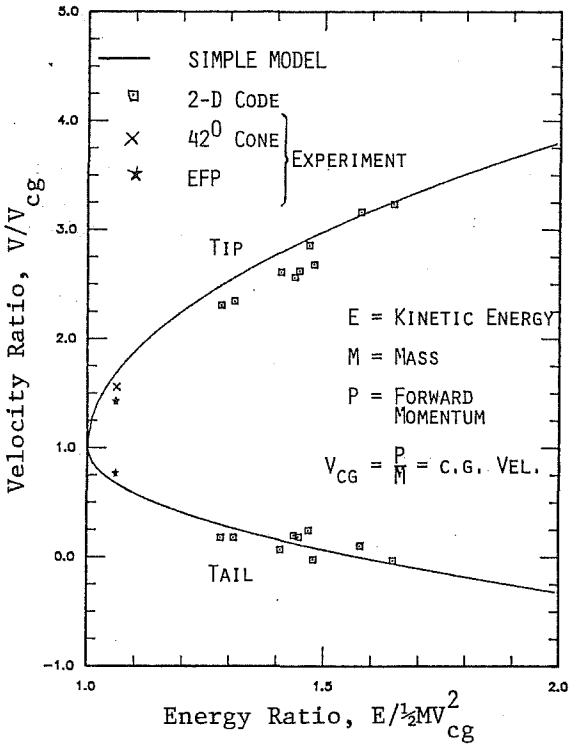

Figure 3. Comparison Between Simple Model and Two-Dimensional Hydrocode for a Ratio of Tip and Tail Radii of 0.25

Included in Figure 3 are a number of points corresponding to jet velocity data predicted by DEFEL. These data are also listed in Table 1. Note that these points are quite close to the curves. Also included are data points from tests of a 42° conical copper shaped charge and a copper self-forging-fragment (SFF) charge. The SFF data fall appreciably inside the curves, probably because the radius ratio was actually somewhat greater than 0.25.

Several observations can be made in this figure. First, the code data fit the curves quite well. This indicates that the assumptions made as to the character of the jet (linear velocity distribution, truncated conical shape, ratio of tip to tail radius) are acceptable, and that mass, momentum, and kinetic energy are indeed constant.

Second, some predicted relationships among jet characteristics may be clearly seen from these curves. For a given average jet velocity V_{CG}, the tip velocity increases and the tail velocity decreases with kinetic energy; that is, stretching rate increases with kinetic energy.

For a warhead of given size, however, experience has shown that the available energy is practically constant. (In fact, code simulations have shown that shaped charges, hemi charges, and self-forging-fragments of the same diameter project jets with kinetic energies within 20% of one another.) In Figure 4, we see that, for jets of equal energy, tip velocity decreases and tail velocity increases with average jet velocity. This may be explained by considering that the jet kinetic energy may be divided into two parts, one associated with the average velocity and the other, the stretching component.

$$E = \frac{1}{2}\int V^2\, dm = \frac{1}{2}\int V_{CG}^2\, dm + \frac{1}{2}\int (V^2 - V_{CG}^2)\, dm \qquad (7)$$

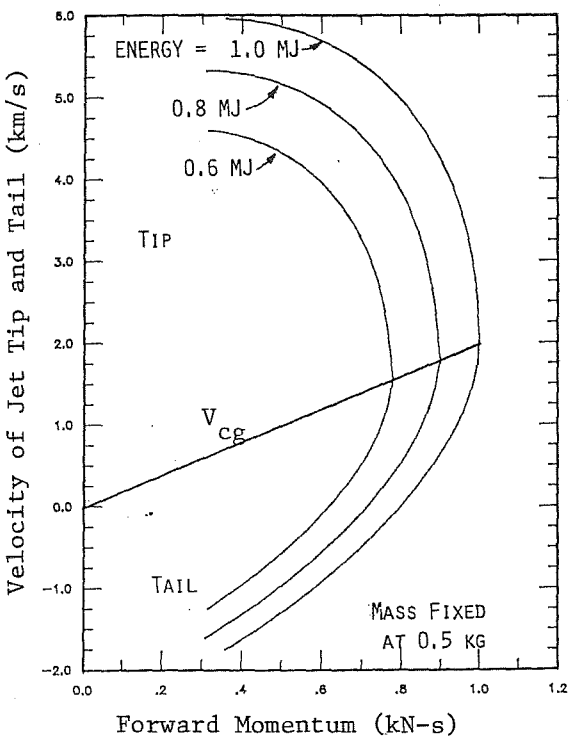

Figure 4. Jet Tip and Tail Velocities as a Function of Total Forward Momentum for Several Values of Jet Kinetic Energy as Predicted by the Model.

Table 1. Data from Hydrocode Simulations of Hemispherical Charges

Design No.	Charge Diam. (mm)	Liner Thickness (mm) Pole	Rim	Kinetic Energy (MJ)	Forward Momentum (kN-s)	Mass (kg)	Velocity (km/s) Tip	Tail	C.G.
L1-A	127	3.3	3.3	0.783	0.643	0.435	4.86	0.00	1.47
L1-B*	127	3.3	3.3	0.873	0.694	0.435	5.11	0.20	1.59
L2-A	127	3.3	1.65	0.861	0.613	0.323	5.18	0.00	1.89
L2-B*	127	3.3	1.65	0.951	0.660	0.323	5.45	0.20	2.04
LD-1	95	2.09	2.09	0.895	0.499	0.178	6.60	0.60	2.79
LD-2	95	2.375	1.425	0.940	0.478	0.159	7.20	0.65	3.00
LD-3	95	2.85	1.425	0.871	0.453	0.169	7.00	0.61	2.68
LD-4	95	3.8	1.9	0.805	0.483	0.212	6.60	0.64	2.27
LD-5	95	2.375	1.1875	0.910	0.439	0.154	7.62	0.61	2.86

*with wave-shaper

When the average velocity is increased, the first term becomes larger. If the total energy is constant, the stretching component must then decrease.

For hemispherical liners, hydrocode simulations indicate that all the liner mass goes into the jet. If the mass of the jet is fixed, and the total kinetic energy is fixed, then the model shows larger total forward momentum, and smaller tip speed, as shown in Figure 4.

The forward momentum is dependent on the liner slope. At one end of the spectrum, the liner is close to a disc, like an SFF liner; all the energy serves to drive the liner forward. As a result, the forward momentum is large, but the difference between jet tip and tail speeds is small, and tip speed is low. The other extreme is a small-angle conical liner (shaped charge), where initially most of the liner energy is in the form of inward radial velocity, and later splits into a fast-moving jet tip, and slow-moving jet tail or slug. The net forward momentum is small. In other words, for fixed total jet mass and kinetic energy, the high tip speed is achieved by driving the liner more inward radially, the high-speed portion of the jet has less mass, and the total forward momentum is small.

This model is primarily for nearly hemispherical liners, but it is also applicable to SEFs. For a non-stretching SFF projectile, with no velocity gradient, the forward momentum is a maximum, as shown in Figure 4 as the extreme right point on each constant-energy curve.

When applying this model to conventional shaped charges with narrow angle cones, there are two ways of accounting for the mass. The total liner mass could be considered, which means that the jet tail is actually the "slug" tail, according to the accepted theory and terminology of [5]. Alternatively, only the mass of the jet may be considered, excluding the mass of the slug.

FORMULAS FOR LINER COLLAPSE

Equations (4) to (6) can be used to predict jet-velocity and radius distributions if the jet's total mass, momentum, and energy are known. These quantities are assumed the same as for the collapsing liner. In this section, formulas for the velocity of each point of the liner are presented. The total momentum and energy will then be obtained by integration.

The nature of the explosive acceleration of a hemispherical liner varies along the liner's contour. Near the liner axis, the problem is similar to the acceleration of a metal plate by a layer of explosive. But near the rim, the situation is closer to the explosive collapse of a cylindrical shell. To predict the velocity of the collapsing hemi liner, then, we shall combine the Gurney formulas for these two problems.

If we denote by V_p the component of liner velocity due to plate acceleration, and by V_c the component due to cylindrical implosion, then the total velocity may be given by:

$$V_{total} = f(\phi)\, V_p + g(\phi)\, V_c \qquad (8)$$

where f and g are functions of the liner polar coordinate ϕ. The total velocity includes only the plate component at the pole, $f(0°) = 1$, $g(0°) = 0$, while at the rim, only the cylindrical component, $f(90°) = 0$, $g(90°) = 1$. Also, over the entire liner, we require that $f(\phi) + g(\phi) = 1$. Several sets of functions satisfying these requirements have been considered here, the most successful of which is

$$f(\phi) = 1 - \sin\phi$$
$$g(\phi) = \sin\phi \qquad (9)$$

The velocity components V_p and V_c are obtained from the appropriate Gurney formulas. The classical formula for a plate is:

$$V_p = \sqrt{2E}\left[\frac{(1 + 2\frac{M}{C_p})^3 + 1}{6(1 + \frac{M}{C_p})} + \frac{M}{C_p}\right]^{-1/2} \quad (10)$$

where E is the Gurney energy, M is the liner mass, and C_p is the explosive mass associated with the plate formula, defined as a cylindrical tube projected axially from the liner element, as in Figure 5.

The other velocity component is given by the cylindrical implosion formula derived by Chanteret [7]:

$$V_c = \sqrt{2E}\left[\left(\frac{R_e^2 - R_i^2}{R_x^2 - R_i^2}\right)\frac{M}{C_c} + \frac{1}{6}\right]^{-1/2} \quad (11)$$

where R_i and R_e are the interior and exterior radii of the explosive, and C_c is the mass of the explosive associated with the cylindrical implosion formula, defined in Figure 5. R_x is the radius of an assumed rigid surface within the explosive, given by:

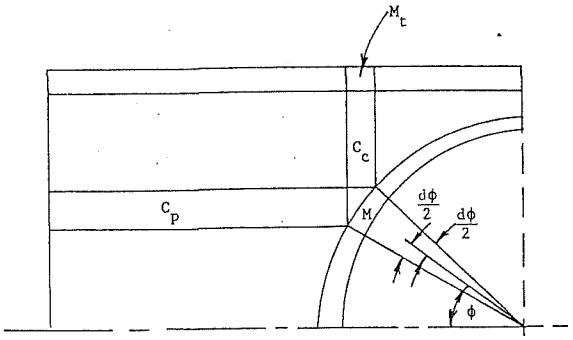

Figure 5. Definition of Metal and Explosive Masses Used in Gurney Formulas.

$$R_x^3 + 3R_x\left[(R_e+R_i)\frac{\rho_o}{\rho_{CJ}}\left(\frac{M}{C_c}R_e + \frac{M_t}{C_c}R_i + R_iR_e\right] - 3(R_i + R_e)R_iR_e\left[\frac{2}{3} + \frac{\rho_o}{\rho_{CJ}}\left(\frac{M}{C_c} + \frac{M_t}{C_c}\right)\right] = 0 \quad (12)$$

This equation may be solved analytically for R_x. M_t is the mass of the confinement (tamping), defined in Figure 5, and ρ_o and ρ_{CJ} are the initial and Chapman-Jouguet densities of the explosive.

The above equations give the magnitude of the velocity, but not its direction. The angle δ of the velocity with respect to the original normal to the liner is given by the unsteady Taylor relation [8]:

$$\delta = \frac{V_o}{2U} - \frac{1}{2}V_o'\tau - \frac{1}{4}V_o\tau' \quad (13)$$

where τ is the characteristic acceleration time of the liner and the primes denote differentiation along the meridian of the liner. Here, we take τ to be a constant, so that the last term vanishes. U is the sweeping velocity of the detonation wave over the liner:

$$U = \frac{U_D}{\cos\gamma} \quad (14)$$

in which U_D is the explosive detonation velocity and γ is the angle between the detonation wavefront and the tangent to the liner.

Once the velocity and direction of collapse are known all along the liner, its mass, momentum, and energy may be found by evaluating the integrals:

$$M = \int_0^{\phi max} 2\pi\rho R_\ell t \sin\phi \, d\phi \quad (15)$$

$$P = \int_0^{\phi max} 2\pi\rho R_\ell t \, V_o \sin\phi \cos(\phi-\delta) d\phi \quad (16)$$

$$E = \int_0^{\phi max} 2\pi\rho R_\ell t \sin\phi \frac{V_o^2}{2} d\phi \quad (17)$$

The mass can be integrated exactly, but the momentum and energy must, in general, be integrated numerically. These quantities may then be substituted into Equations (4) to (6) to determine the properties of the jet.

COMPARISON WITH HYDROCODE CALCULATIONS & EXPERIMENT

As a test of the simplified model, calculated results are compared with other results for actual hemi charges. Table 2 lists tip

Table 2. Comparison of Model with Hydrocode Calculations and Experiments

Liner Thickness (% C.D.)	Confinement	Tip Velocity (km/s) HELP	Exp.	DEFEL	Model	Kinetic Energy (MJ) DEFEL	Model	Momentum (kN-s) DEFEL	Model
3.3	none	4.29	NA	NA	4.15	NA	0.528	NA	0.505
3.3	3.2mm Al	4.39	4.43	4.42	4.41	0.596	0.603	0.572	0.545
3.3	6.4mm St	5.21	4.96	NA	5.00	NA	0.789	NA	0.632
3.0-1.5	3.2mm Al	4.85	4.94	4.64	5.10	0.603	0.607	0.520	0.482
3.0-1.5	6.4mm St	5.95	6.28	NA	5.76	NA	0.781	NA	0.550

velocities for five different charge designs, as simulated by HELP and DEFEL codes, as measured in experiments, and as calculated from the simplified model. The HELP code and experimental data are from BRL [9, 10], and the DEFEL simulations were performed by Dyna East [2, 3]. These charges are all similar to that shown in Figure 2, except for liner tapering and confinement. Included are an unconfined charge with the uniform-wall liner and 6.4-mm-thick-steel-confined charges with the tapered and uniform-wall liners.

The simplified model was first calibrated by adjusting the collapse formulas, Equations (8) and (13), so that the jet kinetic energy (taken as 90% of the collapsing liner's kinetic energy) and axial momentum would agree (as close as possible) with the corresponding properties calculated by the DEFEL code for the aluminum-confined charges. Note that a close match was able to be made with the jet kinetic energy, but that the collapse formula's axial momentum values are 4.7 and 7.3 percent lower than the DEFEL predictions. Once the model was calibrated, calculations of the other three cases were performed.

Comparison of results listed in Table 2 show quite good predictions of tip velocity. The simplified model differs from the HELP results by an average of 3.2% (maximum difference of 5.1%), from the DEFEL results by 5% (10% maximum), and from the experimental results by 3.2% (8.3% maximum). Moreover, trends in tip velocity caused by variations in liner and confinement are reflected in the results of the simplified model. We may conclude that this model can be a useful tool for the designer.

PARAMETRIC STUDY

To further investigate trends in jet properties caused by variations in design parameters, a parametric study was performed. Specifically, variations in liner thickness and tapering, were considered. The 3%-constant-wall copper-lined hemi with thin aluminum confinement shown in Figure 2 was chosen as a baseline about which variations were made.

First, liner thickness was varied over a range of 1.5% to 5% of the charge diameter. Figure 6 shows that, as expected, tip velocity decreases with liner thickness, while Figures 7 and 8 show that total jet momentum and kinetic

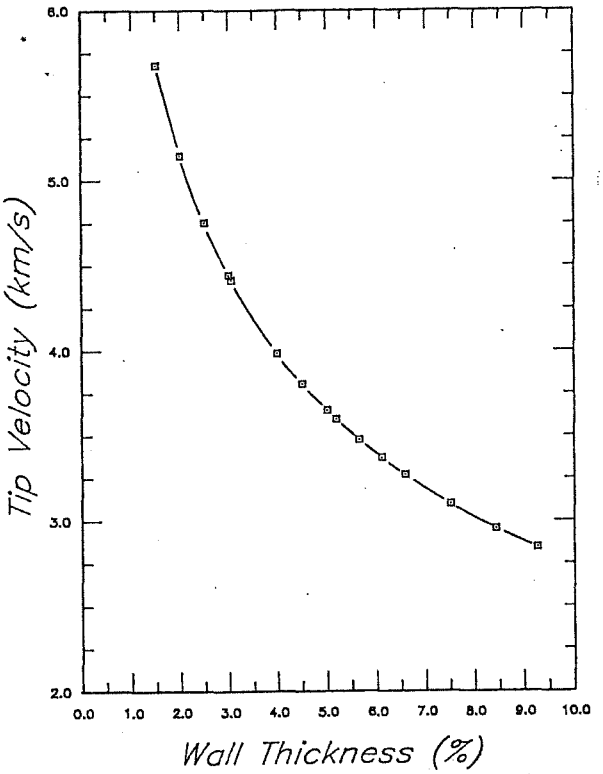

Figure 6. Variation in Jet Tip Velocity with Liner Wall Thickness as Predicted by Simplified Model.

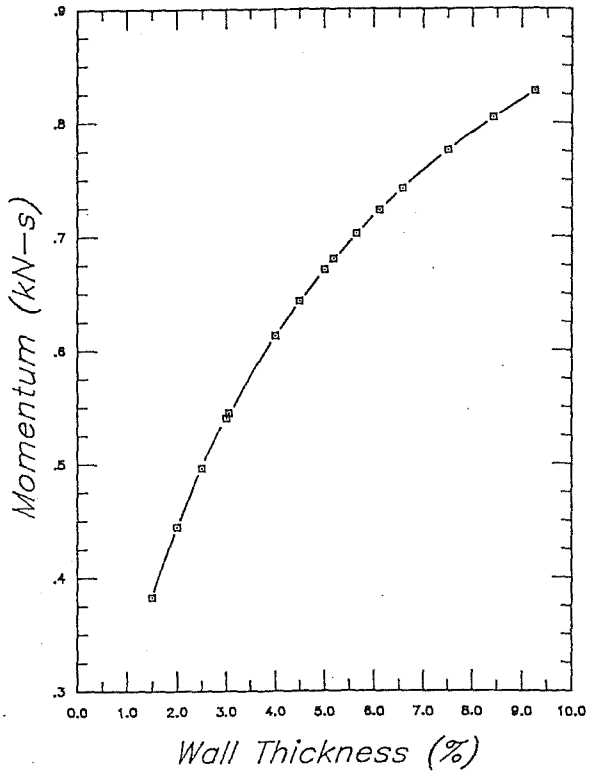

Figure 7. Variation in Jet Axial Momentum with Liner Thickness as Predicted by the Model.

energy increase over this range. This indicates that very thin liners make less efficient use of the available explosive energy. Still, total kinetic energy does not vary a great deal, only about 15% over a three-fold range of liner thickness.

Next, the effect of liner tapering was examined. First, liner thickness at the pole t_p was fixed at 3.3 mm, while thickness at the rim t_e was varied from 1.0 to 4.0 mm. As shown in Figure 9, thinning the rim (increasing the thickness ratio, t_p/t_e) increases tip velocity. As shown in Figure 10, this increase in velocity is gained at the expense of the axial momentum. Jet energy, however, plotted in Figure 11, is not appreciably affected.

Variation of tapering while holding the rim (or equator) thickness fixed was also considered, as included in these three figures. Thickness at the pole was varied over a range of 1.0 to 4.0 mm. Even over this large range, thickening the pole reduces tip velocity

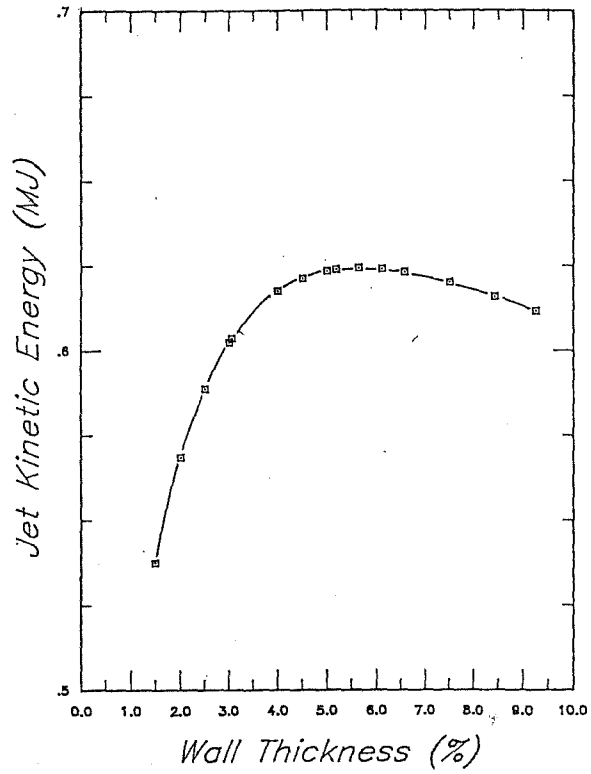

Figure 8. Variation in Jet Kinetic Energy with Liner Wall Thickness as Predicted by Simplified Model.

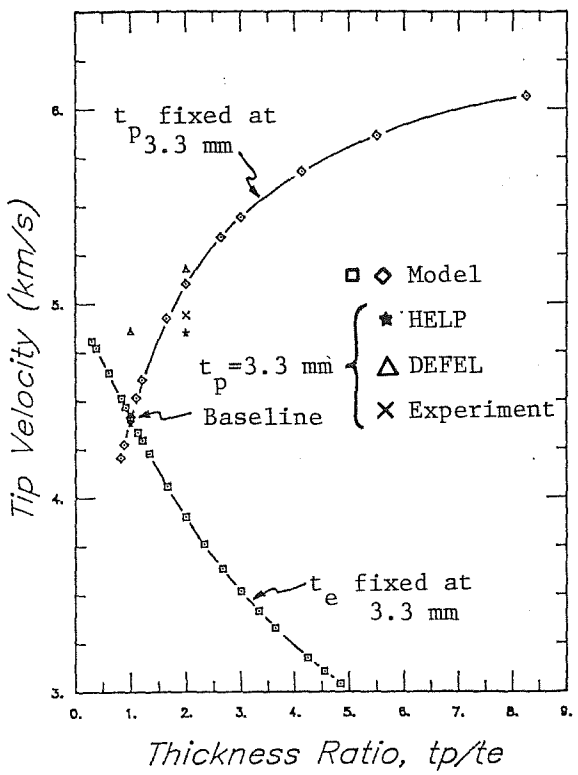

Figure 9. Variation in Jet Tip Velocity with Liner Tapering as Predicted by Simplified Model.

only about 10%, as shown in Figure 9. Figures 10 and 11 show that increasing the pole thickness increases both jet momentum and kinetic energy.

CONCLUSIONS AND DISCUSSIONS

A simplified model based on conservation of mass, momentum, and energy has been developed. With proper selection of the assumed ratio of tip to tail radii, this model gives good agreement with experimentally measured and code-calculated jet velocities. Also, parametric curves generated by the model give insight into the effect of variations in charge configuration on jet properties.

In the model, the ratio of the tip radius to the tail radius was assumed to be a constant. While this may be accurate for a set of charges of largely similar configuration, we have found that for widely differing charges, this ratio can have quite different values. For design purposes, it is recommended that this ratio first be established for the baseline design, and then used in the model to predict the effect of minor design changes.

The collapse formulas presented here represent a simple, mathematical method for coupling the classical Gurney formulas for plate projection and cylindrical implosion for application to a hemispherical liner. While this set of formulas was able to be fit closely to the few cases considered here, a formula based more on physical principles would be more widely applicable.

ACKNOWLEDGMENTS

This research was sponsored by the U.S. Army Ballistic Research Laboratory (BRL). The authors would like to acknowledge Dr. William P. Walters of BRL for his technical guidance and suggestions. They thank Mr. Glenn Weaver, BRL, for providing the results of his code simulations. They also thank Mr. Robert D. Ciccarelli and Mr. Michael Crilly of Dyna East for their analysis of the HELP code calculations.

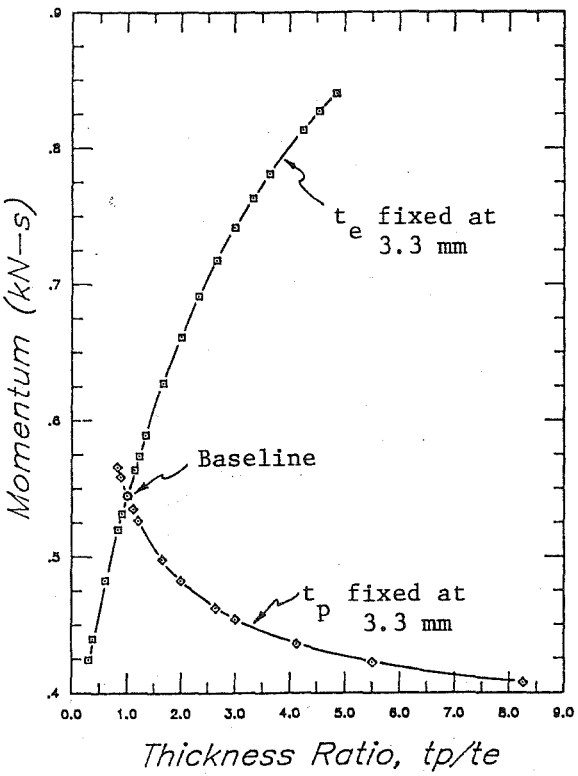

Figure 10. Variation in Jet Axial Momentum with Liner Tapering as Predicted by Simplified Model.

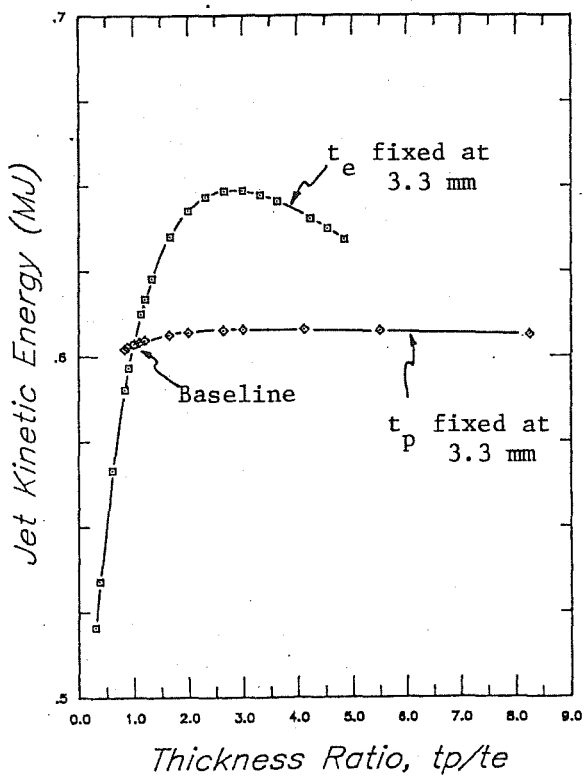

Figure 11. Variation in Jet Kinetic Energy with Liner Tapering as Predicted by Simplified Model.

REFERENCES

[1] Chou, P.C.; Ciccarelli, R.D.; Arbuckle, A.L.; and Walters, W.P., "Jet Formation of an Implosively Loaded Hemispherical Liner," U.S. Army Armament Research and Development Command Contract Report No. ARBRL-CR-00470, September 1981.

[2] Chou, P.C.; Ciccarelli, R.D.; Walters, W.P.; and Weaver, G.W., "Jet Formation Mechanics of Hemispherical Warheads," U.S. Army Armament Research and Development Command Contract Report, to be published.

[3] Chou, P.C.; Ciccarelli, R.D.; and Walters, W.P., "The Formation of Jets from Hemispherical-Liner Warheads," Proc. 7th Int. Symp. on Ballistics, The Hague, Netherlands, 19-21 April 1983.

[4] Flis, W.J.; Miller, S.; and Clark, W.J., "DEFEL: A Finite Element Hydrodynamic Computer Code," Dyna East Corporation DE-TR-84-05, November 1984.

[5] Pugh, E.M.; Eichelberger, R.J.; and Rostoker, N., "Theory of Jet Formation by Charges with Lined Conical Cavities," Journal of Applied Physics, Volume 23, May 1952, pp. 532-536.

[6] Misovec, A.P.; and Garrison, D.R., "Shaped Charge Warheads Utilizing Hemispherical Liners: Analysis of Liner Collapse and Jet Formation," David Taylor Naval Ship Research and Development Center Report No. 76-0088, December 1976.

[7] Chanteret, P.Y., "An Analytical Model for Metal Acceleration by Grazing Detonation," Proc. 7th Int. Symp. on Ballistics, The Hague, Netherlands, 19-21 April 1983.

[8] Chou, P.C., et al., "Improved Formulas for Velocity, Acceleration, and Projection Angle of Explosively Driven Liners," Proc. 6th Int. Symp. of Ballistics, Orlando, Florida, 27-29 October 1981.

[9] Arbuckle, A.L.; Walters, W.P.; and Aseltine, C.L., "Analysis of Uniform Wall and Tapered Hemispherical Liners with Several Explosive Confinement Geometries," Technical Report ARBRL-TR-02222, March 1980.

[10] Walters, W.P., "Experiments with Hemispherical Shaped-Charge Liners," Presented at the ADPA Bombs & Warheads Meeting, 20-21 May 1981, Pensacola, Florida.